



## Hybrid NiCoO<sub>x</sub> adjacent to Pd nanoparticles as a synergistic electrocatalyst for ethanol oxidation

Wei Wang <sup>a, b</sup>, Yan Yang <sup>b</sup>, Yanqin Liu <sup>b</sup>, Zhe Zhang <sup>b</sup>, Wenkui Dong <sup>a,\*</sup>, Ziqiang Lei <sup>b,\*\*</sup>

<sup>a</sup> School of Chemical and Biological Engineering, Lanzhou Jiaotong University, Lanzhou 730070, China

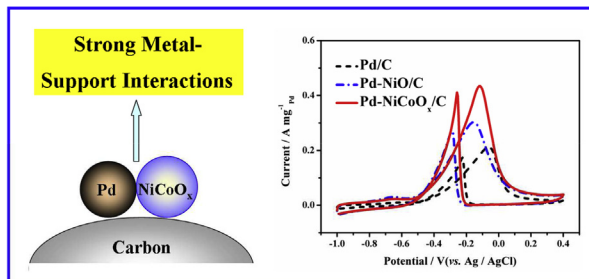
<sup>b</sup> Key Laboratory of Eco-Environment-Related Polymer Materials, Ministry of Education of China, Key Laboratory of Gansu Polymer Materials, College of Chemistry and Chemical Engineering, Northwest Normal University, Lanzhou 730070, China



### HIGHLIGHTS

- Synthesized a novel catalyst with hybrid NiCoO<sub>x</sub> adjacent to Pd.
- SMSI enhanced by the synergistic effect of NiO and CoO<sub>x</sub>.
- Pd-NiCoO<sub>x</sub>/C catalyst has large EASA, high activity and stability.
- Pd-NiCoO<sub>x</sub>/C catalyst exhibits high usage of Pd.

### GRAPHICAL ABSTRACT



### ARTICLE INFO

#### Article history:

Received 8 July 2014

Received in revised form

28 August 2014

Accepted 18 September 2014

Available online 2 October 2014

#### Keywords:

Binary nickel–cobalt oxide

Strong metal-support interactions

Electrocatalysts

Ethanol oxidation

### ABSTRACT

To improve the electrocatalytic activity of Pd for ethanol oxidation, hybrid NiCoO<sub>x</sub> adjacent to Pd catalyst (Pd-NiCoO<sub>x</sub>/C) is successfully synthesized. Physical characterization shows NiCoO<sub>x</sub> is closely adjacent to Pd nanoparticles in Pd-NiCoO<sub>x</sub>/C catalyst, which leads to Strong Metal-Support Interactions (SMSI) between the NiCoO<sub>x</sub> and Pd nanoparticles, in favor of the electrocatalytic properties. The Pd-NiCoO<sub>x</sub>/C catalyst is estimated to own larger electrochemically active surface area than Pd/C and Pd–NiO/C catalysts. Moreover, compared to Pd/C catalyst, the onset potential of Pd-NiCoO<sub>x</sub>/C catalyst is negative 40 mV for ethanol oxidation. Noticeably, the current density of Pd-NiCoO<sub>x</sub>/C catalyst is 2.05 and 1.43 times higher contrasted to Pd/C and Pd–NiO/C catalysts accordingly. Importantly, the Pd-NiCoO<sub>x</sub>/C catalyst exhibits better stability during ethanol oxidation, which is a promising electrocatalyst for application in direct alkaline alcohol fuel cells.

© 2014 Elsevier B.V. All rights reserved.

### 1. Introduction

Up to date, Pd and Pd-based [1–4] electrocatalysts have continued to be research interest for application in direct alkaline alcohol fuel cells (DAAFCs) as a result of following reasons: Pd is more abundant in the earth (at least fifty times more than Pt [5]).

Compared with Pt, Pd possesses high catalytic activity towards ethanol oxidation in alkaline media [6].

However, the electrocatalytic activity and chemical stability of Pd need to be improved. It was reported that these could be achieved by incorporating metal oxides nanoparticles such as ZrO<sub>2</sub>, SnO<sub>2</sub> [7], Co<sub>3</sub>O<sub>4</sub>, NiO [8], Fe<sub>3</sub>O<sub>4</sub> [9] and MnO<sub>2</sub> [10] as cocatalysts. NiO is proved to be a highly efficient cocatalyst among different oxide cocatalysts promoting Pd activity for ethanol oxidation in alkaline [11]. The fact that metal oxides could enhance the electrocatalytic performance of Pd mainly attributes to the following reasons: (i) Metal oxides have been widely used to stabilize the nanoparticles

\* Corresponding author. Tel./fax: +86 931 4938755.

\*\* Corresponding author. Tel./fax: +86 931 7970359.

E-mail addresses: [dongwk@mail.lzjtu.cn](mailto:dongwk@mail.lzjtu.cn) (W. Dong), [leizq@hotmail.com](mailto:leizq@hotmail.com), [wangwchem@163.com](mailto:wangwchem@163.com) (Z. Lei).

against sintering during the catalytic process. (ii) The metal oxides could alter the electronic structure of Pd nanoparticles through the interfacial bonding or electron transfer between Pd and metal oxides [12], which has been named “Strong Metal–Support Interactions” (SMSI) [13]. Unfortunately, the further applications of these metal oxides are hindered by their low electron transfer kinetics and poor electro-active sites. It has been reported that the performance of binary hybrid metal oxides is superior to either of the parent metal oxides [14].

Binary hybrid nickel–cobalt oxide has been investigated as one of the most promising materials for supercapacitors [15], Li-ion batteries [16], optoelectronic devices [17], etc. There is also literature about binary hybrid nickel–cobalt oxide towards O<sub>2</sub> reduction reaction [18], O<sub>2</sub> evolution reaction [19] and methanol oxidation [20]. Comparing with nickel oxide (NiO) and cobaltic oxide (CoO<sub>x</sub>), binary hybrid nickel–cobalt oxide possesses higher conductivity and better electrochemical activity. Nevertheless, no work has been reported about binary hybrid nickel–cobalt oxide for ethanol oxidation in alkaline media.

Binary nickel–cobalt oxide has good electrochemical activity. Nonetheless, it is still no reports to achieve the better electrochemical activity of Pd by incorporating this binary metal oxide for ethanol oxidation. Hence, a novel Pd–NiCoO<sub>x</sub>/C catalyst is synthesized in a facile method and investigated the electrocatalytic activity towards ethanol oxidation in alkaline media. It proves that Pd–NiCoO<sub>x</sub>/C catalyst has better electrochemical activity and stability than Pd–NiO catalyst (For NiO is the best cocatalyst).

## 2. Experimental

### 2.1. Catalyst synthesis

#### 2.1.1. Synthesis of NiCoO<sub>x</sub>/C precursor

The NiCoO<sub>x</sub>/C precursor was synthesized by polyol and heat treatment methods. The NiCl<sub>2</sub>·6H<sub>2</sub>O (101.1 mg) and CoCl<sub>2</sub>·6H<sub>2</sub>O (101.2 mg) were dispersed in round-bottom flask containing 60 mL ethylene glycol (EG), then the C<sub>6</sub>H<sub>3</sub>Na<sub>3</sub>O<sub>7</sub>·6H<sub>2</sub>O (501.1 mg) was added and stirred for 1 h. After that, the carbon black (200.0 mg, Vulcan XC-72R) was put in the flask, stirring and sonicating for half an hour respectively. Subsequently, the flask was removed into oil bath for 4 h at N<sub>2</sub> atmosphere, 180 °C. After cooling to room temperature, the suspension was separated by centrifugation at 8000 rpm for 3 min and washed several times with amounts of deionized water. The product was further dried for 12 h at 50 °C, then, heated at 300 °C for 2 h in muffle furnace in open air. Finally, NiCoO<sub>x</sub>/C precursor was obtained.

#### 2.1.2. Synthesis of Pd–NiCoO<sub>x</sub>/C catalyst

The PdCl<sub>2</sub> (12.1 mg) was dissolved in 30 mL EG, then C<sub>6</sub>H<sub>3</sub>Na<sub>3</sub>O<sub>7</sub>·6H<sub>2</sub>O (40.1 mg) was mixed and stirred for 1 h. After the pH was adjusted to 8 using KOH/EG (5%), 100 mg NiCoO<sub>x</sub>/C precursor was added into the solution, stirring and sonicating for half an hour respectively. Subsequently the suspension was reacted for 4 h in N<sub>2</sub> atmosphere at 180 °C, then centrifuged, washed with deionized water several times and dried at 50 °C for 12 h. Finally, the Pd–NiCoO<sub>x</sub>/C catalyst was obtained. The Pd/C and Pd–NiO/C catalysts were synthesized as references with the similar process.

### 2.2. Characterization

Transmission electron microscopy (TEM) measurements were carried out on an Electron Microscope (FEI TECNAI G<sup>2</sup> TF20 America). X-ray diffraction (XRD) patterns were recorded on a Rigaku D/Max-2400 (Japan) diffractometer, using Cu K<sub>α</sub> radiation operated at 40 kV and 150 mA. X-ray photoelectron spectroscopy (XPS) (Thi-

5702 America) was a monochromatic Al K<sub>α</sub> X-ray source ( $\hbar\nu = 29.35$  eV).

The electrochemical experiments were performed using an Autolab electrochemical work station (PGSTAT128N, Eco Chemie, Netherlands). A conventional three-electrode cell was used, including an Ag/AgCl electrode as the reference, a platinum wire as the counter, and a modified glass carbon (5 mm in diameter) as the working electrode. The working electrode was prepared as follows: 5 mg catalyst was dispersed ultrasonically in 1 mL Nafion/ethanol (0.25% Nafion). 8 μL suspensions were quantitatively transferred to the surface of polished glassy carbon electrode, followed by drying in air. Before each measurement, the solution was purged with high-purity N<sub>2</sub> gas for at least 30 min to ensure the gas saturated.

## 3. Results and discussion

Nanocomposites containing two or more different nanoscale functionalities are attractive candidates for advanced nanomaterials [21]. Therefore, the Pd–NiCoO<sub>x</sub>/C catalyst was synthesized by epitaxial growth of Pd nanoparticles onto oxidized NiCo alloy. The synthesis procedure is schematically represented in Fig. 1. NiCoO<sub>x</sub>/C precursor was synthesized by polyol and heat treatment methods. Firstly, in the presence of nickel (II) salt, cobalt (II) salt and ethylene glycol (as a solvent and reductant), the supported NiCo alloy nanoparticles were obtained. Secondly, NiCo alloy nanoparticles were transformed into NiCoO<sub>x</sub>/C precursor by heating at 300 °C for 2 h in muffle furnace in open air. Finally, with the former polyol method, palladium (II) salt was reduced to Pd nanoparticles onto the NiCoO<sub>x</sub>/C precursor, forming Pd–NiCoO<sub>x</sub>/C catalyst that hybrid NiCoO<sub>x</sub> was adjacent to Pd nanoparticles.

### 3.1. Physical characterization

The morphology and particle size of Pd–NiCoO<sub>x</sub>/C catalyst are investigated by applying TEM in Fig. 2. Uniform supported nanoparticles are clearly observed on the carbon in TEM image of Fig. 2a without agglomerating. These nanoparticles are in the range of 2–10 nm and the average particle size is around 4.8 ± 0.4 nm

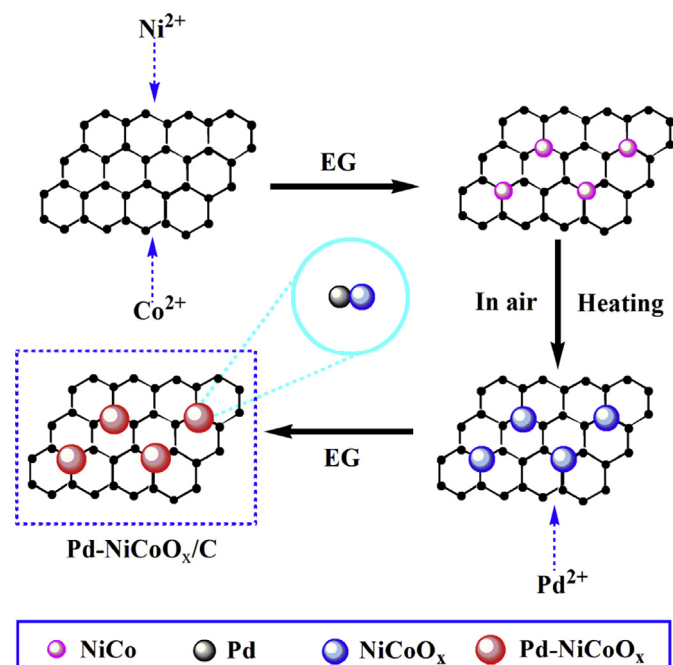
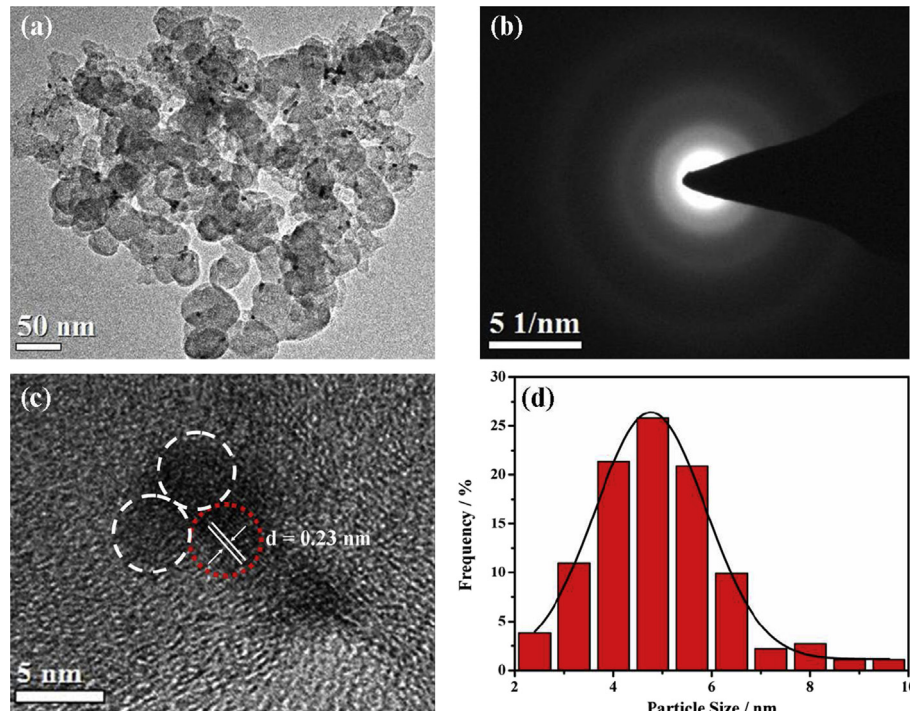


Fig. 1. Schematic synthesis of Pd–NiCoO<sub>x</sub>/C catalyst.



**Fig. 2.** Typical morphology of Pd-NiCoO<sub>x</sub>/C catalyst: (a) The TEM image. (b) The corresponded SAED patterns. (c) High magnification TEM image. (d) Size distribution histograms.

(Fig. 2d). Furthermore, the Pd-NiCoO<sub>x</sub>/C catalyst is confirmed to be a typical face-centered cubic (*fcc*) polycrystalline structure by selected area electron diffraction (SAED) pattern (Fig. 2b). Meanwhile, the lattice fringe in the area expressed by dots (Fig. 2c) with an interplanar spacing of 0.23 nm is associated with Pd (111) lattice fringes [22]. In addition, the NiCoO<sub>x</sub> adjacent to Pd may be amorphous because no clear lattice fringe can be seen in the dashed zone [23]. Apparently, closely joint interfaces are created between the NiCoO<sub>x</sub> and Pd nanoparticles in Pd-NiCoO<sub>x</sub>/C catalyst, which will lead to a stronger SMSI between NiCoO<sub>x</sub> and Pd nanoparticles confirmed by the following XPS measurement, in favor of the electrocatalytic properties [24].

XRD measurement is conducted to obtain the crystallographic information of catalyst. As displayed in Fig. 3a, the characteristic diffraction peak at about 24.8° in all the XRD patterns belongs to the graphite (200) plane of carbon support, and four typical diffraction peaks at 40.1°, 46.4°, 68.2°, and 81.8° in the XRD pattern of Pd/C, corresponding to the (111), (200), (220) and (311) planes of face-

centered cubic (*fcc*) crystalline structure of Pd respectively, consistent with the TEM observation [25,26]. The (111) peaks of Pd are obvious for all catalysts, and the Pd (111) diffraction peak of Pd-NiCoO<sub>x</sub>/C shows no obvious shift with respect to that of Pd-NiO/C and Pd/C, indicating that oxide has no effect on the crystalline of Pd. Moreover, evaluating the ratio of peak intensity for Pd (111) and C (200) crystal faces [27], the relative crystallinity of Pd-NiO/C and Pd-NiCoO<sub>x</sub>/C catalyst are smaller than Pd/C catalyst. At the same time, no peak is observed for NiCoO<sub>x</sub> nanoparticles in the Pd-NiCoO<sub>x</sub>/C catalyst, predicated that NiCoO<sub>x</sub> is most likely present in the form of the amorphous species [28].

To analyze the underlying interfacial interaction between Pd and NiCoO<sub>x</sub> nanoparticles, XPS is employed to probe the electronic properties of the Pd-NiCoO<sub>x</sub>/C catalyst. Fig. 3b shows the Pd 3d XPS spectra of the Pd-NiCoO<sub>x</sub>/C and Pd/C. The Pd 3d<sub>5/2</sub> and Pd 3d<sub>3/2</sub> peaks of Pd-NiCoO<sub>x</sub>/C (335.8 eV, 341.2 eV) are 0.4 eV and 0.6 eV negative compared to Pd/C (335.4 eV, 340.6 eV), respectively. This significant shift is apparently ascribed to the strong electronic

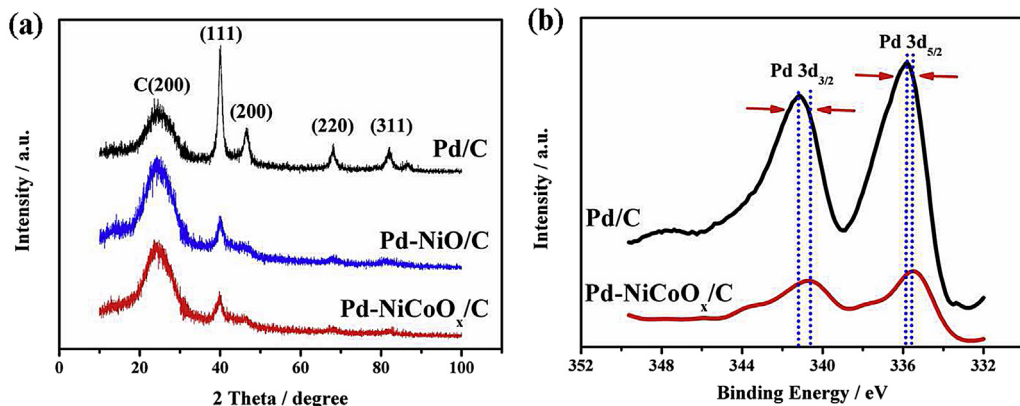


**Fig. 3.** (a) XRD patterns of Pd/C, Pd-NiO/C and Pd-NiCoO<sub>x</sub>/C catalysts. (b) Pd 3d XPS spectrums of Pd/C and Pd-NiCoO<sub>x</sub>/C catalysts.

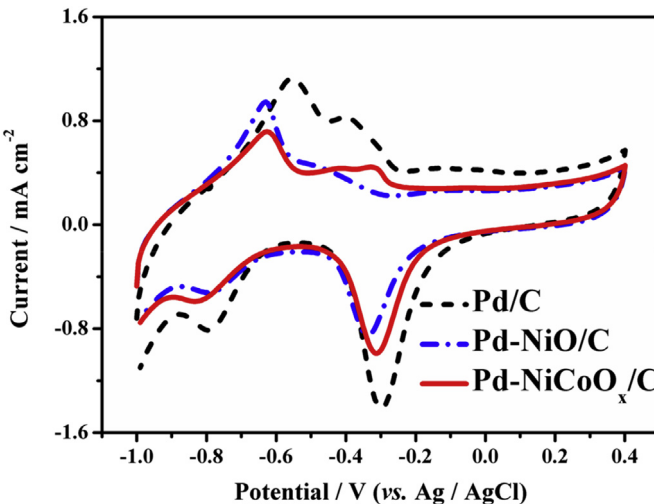


**Fig. 4.** Cyclic voltammograms of Pd/C, Pd–NiO/C and Pd–NiCoO<sub>x</sub>/C catalysts in N<sub>2</sub>-saturated 0.1 M KOH. Scan rate: 50 mV s<sup>-1</sup>.

interaction between Pd and NiCoO<sub>x</sub> nanoparticles, indicating the obvious electron transfer from Pd to NiCoO<sub>x</sub>. Such observation has also been reported, this electron transfer will reduce the d-band center of the metals and thus the adsorption energy of the poisoning intermediates on the metal surfaces, which would contribute positively to the removal of the poisoning intermediate, thus enhancing the electrocatalytic performance for ethanol oxidation [24,29].

### 3.2. Electrochemical measurements

Electrochemical measurements on Pd–NiCoO<sub>x</sub>/C catalyst were implemented as follows. Fig. 4 shows the electrochemical response of Pd/C, Pd–NiO/C and Pd–NiCoO<sub>x</sub>/C catalysts in 0.1 M KOH solution in the potential between −1.0 V and 0.4 V (vs. Ag/AgCl) at a scan rate of 50 mV s<sup>-1</sup>. The anodic peaks of Pd/C at −0.58 V, −0.40 V and −0.10 V (vs. Ag/AgCl) correspond to hydrogen desorption, OH-adsorption and Pd oxide formation, accordingly. And the cathodic peaks of −0.30 V and −0.80 V (vs. Ag/AgCl) are assigned to the reduction of Pd oxide and hydrogen adsorption/absorption [30]. The cyclic voltammograms of Pd–NiO/C and Pd–NiCoO<sub>x</sub>/C catalysts are mainly similar to the Pd/C except the locations and sizes of the characteristic peaks show a little of difference owing to the presence of metal oxides nanoparticles [31,32].

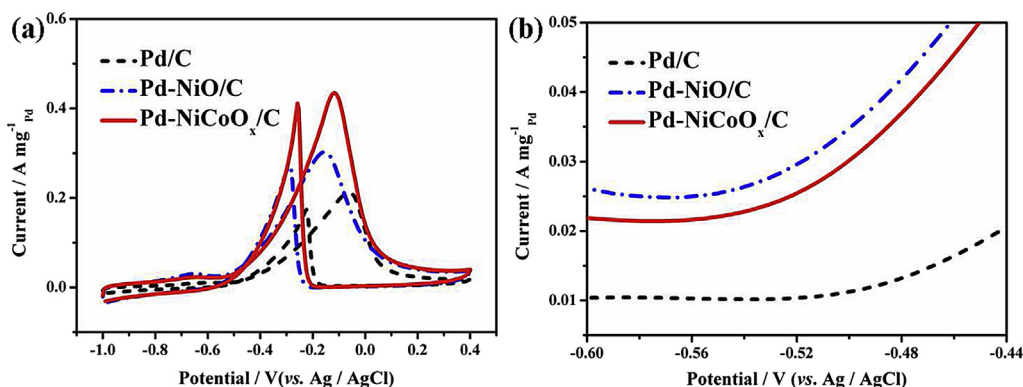


**Fig. 5.** (a) Cyclic voltammograms of Pd/C, Pd–NiO/C and Pd–NiCoO<sub>x</sub>/C catalysts in N<sub>2</sub>-saturated 0.1 M KOH + 0.5 M C<sub>2</sub>H<sub>5</sub>OH and (b) magnified potential window from −0.60 V to −0.44 V. Scan rate: 50 mV s<sup>-1</sup>.

As the activity of a catalyst is not only controlled by intrinsic properties but also by the surface area. The electrochemically active surface area (EASA) of catalyst has been measured by determining the coulombic charge for the reduction of palladium oxide according to Eq. (1) [33]:

$$\text{EASA} = Q/SI \quad (1)$$

$Q$  is the coulombic charge for the reduction of Pd oxide in mC;  $S$  is a proportionality constant used to relate charge with area;  $I$  is the catalyst loading in mg.

A charge value of 0.405 mC cm<sup>-2</sup> is assumed for the reduction of a PdO monolayer [34]. The EASA values are estimated to be 298.15 cm<sup>2</sup> mg<sup>-1</sup>Pd, 482.85 cm<sup>2</sup> mg<sup>-1</sup>Pd and 589.85 cm<sup>2</sup> mg<sup>-1</sup>Pd for Pd/C, Pd–NiO/C and Pd–NiCoO<sub>x</sub>/C, respectively. The highest value is obtained for Pd–NiCoO<sub>x</sub>/C among the three catalysts. Because the value of EASA could reveal the utilization of Pd [35], this result also implies a good utilization of Pd with the assistance of close contacted NiCoO<sub>x</sub> nanoparticles.

Then the electrocatalytic performance of the Pd–NiCoO<sub>x</sub>/C for ethanol oxidation was investigated in N<sub>2</sub>-saturated 0.1 M KOH with 0.5 M C<sub>2</sub>H<sub>5</sub>OH solution by cyclic voltammetry. As shown in Fig. 5a, each curve appears two oxidation current peaks, one in the forward scan and the other in the reverse scan. In the forward scan, the oxidation peak (about −0.1 V vs. Ag/AgCl) is assigned to the oxidation of freshly chemisorbed species coming from ethanol adsorption. Whereas, the oxidation peak in the reverse scan (about −0.3 V vs. Ag/AgCl) is primarily associated with the removal of carbonaceous species not completely oxidized in the forward scan [36]. Notably, the current density of oxidation peak at −0.1 V (vs. Ag/AgCl) for Pd–NiCoO<sub>x</sub>/C catalyst (0.43 A mg<sup>-1</sup>Pd) is 2.05 and 1.43 times higher compared to Pd/C (0.21 A mg<sup>-1</sup>Pd) and Pd–NiO/C (0.30 A mg<sup>-1</sup>Pd) catalysts respectively. It demonstrates NiCoO<sub>x</sub> could more effectively enhance the electrochemical activity of Pd than NiO for ethanol oxidation. Meanwhile, Fig. 5b presents that the onset potential of Pd–NiCoO<sub>x</sub>/C (−0.56 V vs. Ag/AgCl) is similar to that of Pd–NiO/C for ethanol oxidation, which shows that NiCoO<sub>x</sub> and NiO have same effect on the nucleation and crystallization of Pd nanoparticles. Moreover, the onset potential of Pd–NiCoO<sub>x</sub>/C is more negative in contrast with Pd/C (−0.52 V vs. Ag/AgCl). It is also well known that the more negative the onset potential is, the higher trend of ethanol oxidation will be. Based on the above results, the Pd–NiCoO<sub>x</sub>/C catalyst has good activity for ethanol oxidation, verifying the function of SMSI between the NiCoO<sub>x</sub> and Pd nanoparticles in TEM and XPS characterizations.

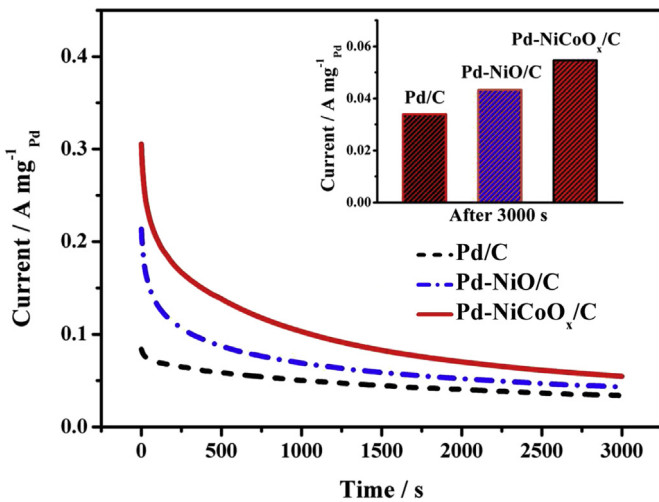


**Fig. 6.** Chronoamperometric curves of ethanol oxidation on the Pd/C, Pd–NiO/C and Pd–NiCoO<sub>x</sub>/C catalysts for 3000 s. Fixed potential: −0.2 V (vs. Ag/AgCl). The insert: Current of catalysts after 3000 s.

The longtime stability of catalyst is very important in the application of DAAFCs. Since the poisoning of electrocatalyst due to the formation of oxidation intermediates, particularly CO, leads to the recession of activity. Therefore, the stability is also researched by chronoamperometry at the potential of −0.2 V (vs. Ag/AgCl). Fig. 6 shows that current densities of all catalysts are gradually reduced as the time increased, indicating the poisoning of electrocatalysts. But at any time, the current density of catalysts is following the order: Pd–NiCoO<sub>x</sub>/C > Pd–NiO/C > Pd/C. Furthermore, the current density on Pd–NiCoO<sub>x</sub>/C catalyst (0.055 A mg<sup>-1</sup>Pd) after 3000 s is higher than that on Pd–NiO/C (0.043 A mg<sup>-1</sup>Pd) and Pd/C

(0.034 A mg<sup>-1</sup>Pd) catalysts. (Inserted in Fig. 6) It clearly demonstrates a good stability of the Pd–NiCoO<sub>x</sub>/C catalyst.

Moreover, the mechanism of ethanol oxidation on Pd–NiCoO<sub>x</sub>/C was preliminary studied. The curve of linear sweep voltammatic approximates the steady-state polarization curve under a slow scan rate, which reflects kinetic processes of ethanol oxidation in some degree. Fig. 7a shows the evolutions in N<sub>2</sub>-saturated 0.1 M KOH with 0.5 M C<sub>2</sub>H<sub>5</sub>OH solution on Pd/C, Pd–NiO/C and Pd–NiCoO<sub>x</sub>/C catalysts at a scan rate of 1 mV s<sup>-1</sup>. In low potential (below −0.4 V vs. Ag/AgCl), the current of all catalysts increases slowly with the increase of polarization potential. However, the current increases sharply as the potential increasing, and the Pd–NiCoO<sub>x</sub>/C catalyst is greater than that of the Pd–NiO/C and Pd/C catalysts in high potential (above −0.4 V vs. Ag/AgCl). According to Fig. 7a, Tafel plots on these catalysts are illustrated in Fig. 7b, c and d. Tafel slopes derived from the linear region (from −0.4 V to −0.2 V (vs. Ag/AgCl)) are divided into two parts. The first slope values are 174.6 mV dec<sup>-1</sup> and 179.5 mV dec<sup>-1</sup> for Pd–NiO/C and Pd–NiCoO<sub>x</sub>/C respectively in the potential of −0.4 V to −0.35 V (vs. Ag/AgCl), which are lower than that of Pd/C (239.8 mV dec<sup>-1</sup>). Upon lower Tafel slopes, the charge-transfer kinetics on Pd–NiO/C and Pd–NiCoO<sub>x</sub>/C catalysts is faster than Pd/C for ethanol oxidation [35]. While for Pd/C, Pd–NiO/C and Pd–NiCoO<sub>x</sub>/C, the second Tafel slopes in the potential of −0.35 V to −0.2 V (vs. Ag/AgCl) are 344.0 mV dec<sup>-1</sup>, 296.7 mV dec<sup>-1</sup>, 282.9 mV dec<sup>-1</sup> accordingly. The second slopes are different from the first ones, which indicate the mechanism of ethanol oxidation has changed. The kinetics of ethanol oxidation is dominated by the adsorption on hydroxyl in the low-potential region from −0.4 V to −0.35 V (vs. Ag/AgCl), and further affected by the formation of the inactive oxide layer on the Pd at potentials above −0.3 V (vs. Ag/AgCl) [37].

To understand more about the good performance of the Pd–NiCoO<sub>x</sub>/C catalyst, ethanol oxidation experiments on the Pd/C and

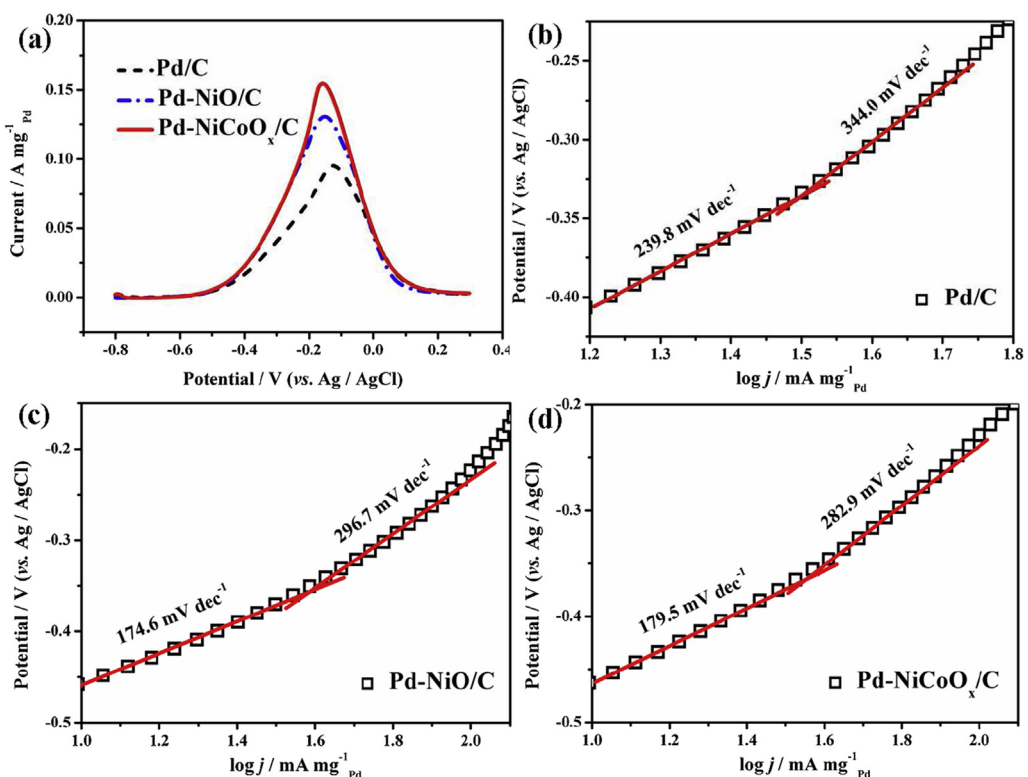


**Fig. 7.** (a) Linear sweep voltammograms of Pd/C, Pd–NiO/C and Pd–NiCoO<sub>x</sub>/C catalysts in N<sub>2</sub>-saturated 0.1 M KOH + 0.5 M C<sub>2</sub>H<sub>5</sub>OH. (b) (c) (d) Corresponded Tafel plots. Scan rate: 1 mV s<sup>-1</sup>.

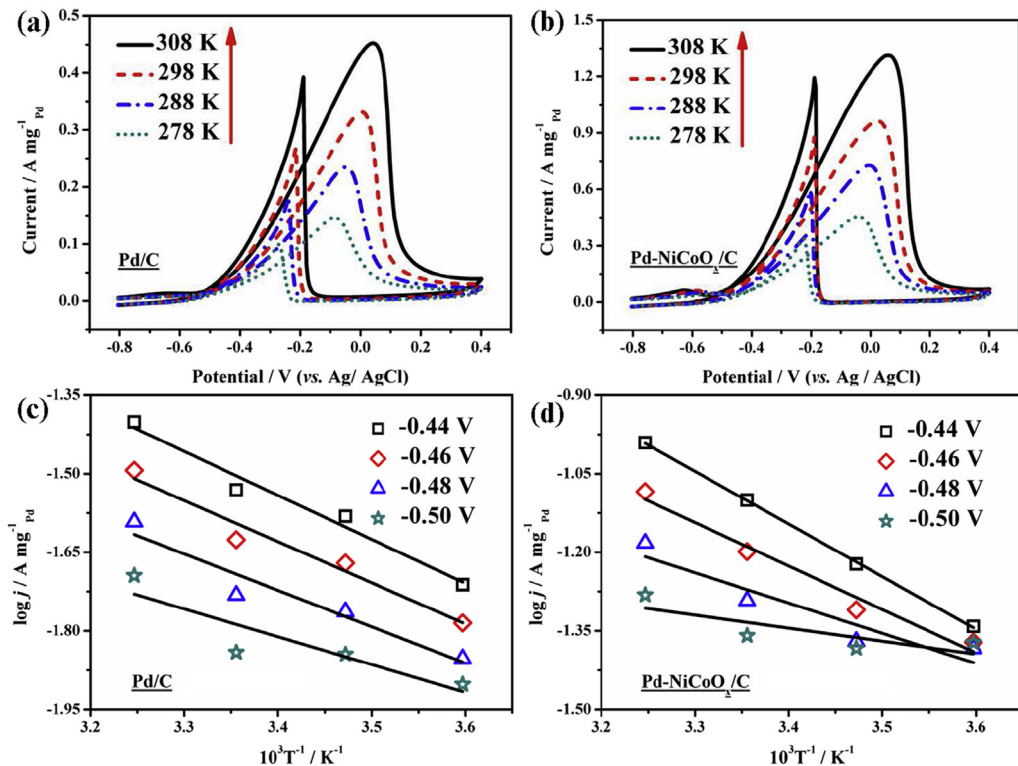


**Fig. 8.** Cyclic voltammograms of Pd/C (a) and Pd-NiCoO<sub>x</sub>/C (b) in N<sub>2</sub>-saturated 0.1 M KOH + 0.5 M C<sub>2</sub>H<sub>5</sub>OH at different temperatures. Scan rate: 50 mV s<sup>-1</sup>. Arrhenius plots on Pd/C (c) and Pd-NiCoO<sub>x</sub>/C (d) catalysts.

Pd-NiCoO<sub>x</sub>/C catalysts were also performed within the temperature range of 278–308 K. Fig. 8a and b displays increasing oxidation current with rising temperature, which proves the process is thermally activated. Meanwhile, it is found that the current density on Pd-NiCoO<sub>x</sub>/C catalyst is always larger than that on Pd/C at the same temperatures. It further demonstrates that Pd-NiCoO<sub>x</sub>/C has better electrocatalytic performance. Additionally, an apparent activation energy value can be calculated according to Eq. (2) [38]:

$$\log j = \log A - E_a / 2.3RT \quad (2)$$

*j* is the current at a specific potential;

*R* is the gas constant;

*T* is the temperature in K;

*E<sub>a</sub>* is the apparent activation energy.

By linearly fitting log *j* and *T*<sup>-1</sup>, it can be obtained from Fig. 8c and d that the *E<sub>a</sub>* for Pd/C and Pd-NiCoO<sub>x</sub>/C is 13.6 ± 0.5 kJ mol<sup>-1</sup> and 12.7 ± 0.3 kJ mol<sup>-1</sup>, respectively. The *E<sub>a</sub>* is smaller, the less energy-consuming and the more conducive to reaction in theory. Therefore, the result further demonstrates that the Pd-NiCoO<sub>x</sub>/C catalyst has better intrinsic property for ethanol than Pd/C.

As the contents of Ni in Pd–NiO/C and NiCo in Pd–NiCoO<sub>x</sub>/C are same, the enhanced electrocatalytic activity of Pd–NiCoO<sub>x</sub>/C catalyst may result from the binary hybrid NiCoO<sub>x</sub>. The reasons are considered that: (i) Oxide functions in Pd–NiCoO<sub>x</sub>/C catalyst because OH<sub>ad</sub> species could easily form on the surface of oxide. The formed OH<sub>ad</sub> species at lower potentials can transform CO-like or other carbonaceous species on the surface of Pd to CO<sub>2</sub>, releasing the active sites on Pd for further reaction. Moreover, oxide on the surface of Pd nanoparticles could also help to break C–C bond [11,39]. A synergistic effect of NiO and CoO<sub>x</sub> in NiCoO<sub>x</sub> facilitates the formation of OH<sub>ad</sub> species and accelerates the breakage of C–C

bond. (ii) The SMSI between Pd and NiCoO<sub>x</sub> nanoparticles is stronger than that of NiO, forming smaller Pd nanoparticles, which leads to a larger EASA, providing more active sites than that of Pd–NiO/C catalyst. Therefore, the performance of Pd–NiCoO<sub>x</sub>/C catalyst is better than that of Pd–NiO/C catalyst for ethanol oxidation. Further study on the optimal ratio of Ni and Co and the load of Pd will be carried out in near future.

#### 4. Conclusion

In summary, Pd–NiCoO<sub>x</sub>/C catalyst has been successfully synthesized via epitaxial growth of Pd nanoparticles onto oxidized NiCo alloy (NiCoO<sub>x</sub>) and introduced to the ethanol oxidation in alkaline. The Pd–NiCoO<sub>x</sub> catalyst exhibits good electrocatalytic performances, including large EASA, high current density and stability for ethanol oxidation. Noticeably, the current density of Pd–NiCoO<sub>x</sub>/C catalyst is 2.05 and 1.43 times higher contrasted to Pd/C and Pd–NiO/C catalysts accordingly. Moreover, the onset potential of Pd–NiCoO<sub>x</sub>/C catalyst is negative 40 mV than the Pd/C for ethanol oxidation. In addition, kinetic and thermodynamic studies reveal that the Pd–NiCoO<sub>x</sub>/C catalyst has lower Tafel slope and *E<sub>a</sub>*, leading to a superior charge transfer rate and a lower energy barrier towards ethanol oxidation. The improved electrocatalytic activity of Pd–NiCoO<sub>x</sub>/C catalyst mainly ascribes to the synergistic effect of NiO and CoO<sub>x</sub> to Pd, producing SMSI between binary hybrid NiCoO<sub>x</sub> and Pd nanoparticles. Considering the good performance of Pd–NiCoO<sub>x</sub> catalyst, it is a promising catalyst for catalytic applications in DAAFCs.

#### Acknowledgment

We thank to the National Natural Science Foundation of China (NO. 21174114), the Program for Changjiang Scholars and

Innovative Research Team in University (IRT1177), Key Laboratory of Eco-Environment-Related Polymer Materials of Ministry of Education, and Key Laboratory of Polymer Materials of Gansu Province.

## References

- [1] V. Mazumder, M. Chi, M.N. Mankin, Y. Liu, O. Metin, D. Sun, K.L. More, S. Sun, *Nano Lett.* 12 (2012) 1102–1106.
- [2] Y.W. Lee, M. Kim, Y. Kim, S.W. Kang, J.H. Lee, S.W. Han, *J. Phys. Chem. C* 114 (2010) 7689–7693.
- [3] C.W. Xu, H. Wang, P.K. Shen, S.P. Jiang, *Adv. Mater.* 19 (2007) 4256–4259.
- [4] S.T. Nguyen, H.M. Law, H.T. Nguyen, N. Kristian, S. Wang, S.H. Chan, X. Wang, *Appl. Catal. B Environ.* 91 (2009) 507–515.
- [5] O. Savadogo, K. Lee, K. Oishi, S. Mitsushima, N. Kamiya, K.I. Ota, *Electrochem. Commun.* 6 (2004) 105–109.
- [6] Y. Wang, X. Wang, C.M. Li, *Appl. Catal. B Environ.* 99 (2010) 229–234.
- [7] K. Sekizawa, H. Widjaja, S. Maeda, Y. Ozawa, K. Eguchi, *Catal. Today* 59 (2000) 69–74.
- [8] M. Wang, W. Liu, C. Huang, *Int. J. Hydrogen Energy* 34 (2009) 2758–2764.
- [9] S. Chen, R. Si, E. Taylor, J. Janzen, J. Chen, *J. Phys. Chem. C* 116 (2012) 12969–12976.
- [10] Y. Zhao, L. Zhan, J. Tian, S. Nie, Z. Ning, *Int. J. Hydrogen Energy* 35 (2010) 10522–10526.
- [11] C. Xu, Z. Tian, P. Shen, S.P. Jiang, *Electrochim. Acta* 53 (2008) 2610–2618.
- [12] J.A. Farmer, C.T. Campbell, *Science* 329 (2010) 933–936.
- [13] A. Kumar, V. Ramani, *ACS Catal.* 4 (2014) 1516–1525.
- [14] J. Landon, E. Demeter, N. Inoglu, C. Keturakis, I.E. Wachs, R. Vasić, A.I. Frenkel, J.R. Kitchin, *ACS Catal.* 2 (2012) 1793–1801.
- [15] Z. Wang, Y. Zhang, Y. Li, H. Fu, *RSC Adv.* 4 (2014) 20234–20238.
- [16] J. Li, S. Xiong, Y. Liu, Z. Ju, Y. Qian, *ACS Appl. Mater. Interfaces* 5 (2013) 981–988.
- [17] L. Hu, L. Wu, M. Liao, X. Fang, *Adv. Mater.* 23 (2011) 1988–1992.
- [18] G. Zhang, B.Y. Xia, X. Wang, X.W. Lou, *Adv. Mater.* 26 (2014) 2408–2412.
- [19] L. Trotchaud, J.K. Ranney, K.N. Williams, S.W. Boettcher, *J. Am. Chem. Soc.* 134 (2012) 17253–17261.
- [20] R. Ding, L. Qi, M. Jia, H. Wang, *Catal. Sci. Technol.* 3 (2013) 3207–3215.
- [21] H. Yu, M. Chen, P.M. Rice, S.X. Wang, R.L. White, S. Sun, *Nano Lett.* 5 (2005) 379–382.
- [22] A.J. Wang, F.F. Li, J.N. Zheng, H.X. Xi, Z.Y. Meng, J.J. Feng, *RSC Adv.* 3 (2013) 10355–10362.
- [23] Z. Zhuang, W. Sheng, Y. Yan, *Adv. Mater.* 26 (2014) 3950–3955.
- [24] Q. Tan, C. Du, Y. Sun, G. Yin, Y. Gao, *J. Mater. Chem. A* 2 (2014) 1429–1435.
- [25] C. Hu, Y. Guo, J. Wang, L. Yang, Z. Yang, Z. Bai, J. Zhang, K. Wang, K. Jiang, *ACS Appl. Mater. Interfaces* 4 (2012) 4461–4464.
- [26] Z. Liu, X. Zhang, L. Hong, *Electrochem. Commun.* 11 (2009) 925–928.
- [27] R. Wang, H. Li, H. Feng, H. Wang, Z. Lei, *J. Power Sources* 195 (2010) 1099–1102.
- [28] C. Jin, X. Sun, Z. Chen, R. Dong, *Mater. Chem. Phys.* 135 (2012) 433–437.
- [29] M. Itoh, M. Saito, M. Takehara, K. Motoki, J. Iwamoto, K. Machida, *J. Mol. Catal. A Chem.* 304 (2009) 159–165.
- [30] F. Gobal, R. Arab, *J. Electroanal. Chem.* 647 (2010) 66–73.
- [31] R.S. Amin, R.M. Abdel-Hameed, K.M. El-Khatib, M. Elsayed-Youssef, *Int. J. Hydrogen Energy* 39 (2014) 2026–2041.
- [32] Q.L. Zhang, J.N. Zheng, T.Q. Xu, A.J. Wang, J. Wei, J.R. Chen, J.J. Feng, *Electrochim. Acta* 132 (2014) 551–560.
- [33] R.N. Singh, R. Awasthi, *Catal. Sci. Technol.* 1 (2011) 778–783.
- [34] O.O. Fashedemila, K.I. Ozoemena, *Phys. Chem. Chem. Phys.* 15 (2013) 20982–20991.
- [35] M.S. Ahmed, S. Jeon, *ACS Catal.* 4 (2014) 1830–1837.
- [36] R.N. Singh, A. Singh, Anindita, *Carbon* 47 (2009) 271–278.
- [37] Z.X. Liang, T.S. Zhao, J.B. Xu, L.D. Zhu, *Electrochim. Acta* 54 (2009) 2203–2208.
- [38] A. Velázquez-Palenzuela, F. Centellas, J.A. Garrido, C. Arias, R.M. Rodríguez, E. Brillas, P.L. Cabot, *J. Power Sources* 196 (2011) 3503–3512.
- [39] C. Xu, P.K. Shen, *Chem. Commun.* 19 (2004) 2238–2239.